LOGIC
Journal of Engineering Design and Technology
Vol. 25 No.3 November; p. 210-218

p-ISSN : 1412-114X
e-ISSN : 2580-5649
http://ojs2.pnb.ac.id/index.php/LOGIC

THERMAL PERFORMANCE OF A BRANCHING-CHANNEL LIQUID COOLING SYSTEM FOR CYLINDRICAL LI-ION 18650 BATTERIES

Anggie Topan Wijaya[1)], James Julian[1)*], Fitri Wahyuni[1)], Riki Hendra Purba[1)], Fathin Muhammad Mahdhudhu[2)], Elvi Armadani[3)], Adi Winarta[4)]

1) Mechanical Engineering, Universitas Pembangunan Nasional Veteran Jakarta, Jakarta
2) Naval Architecture, Universitas Pembangunan Nasional Veteran Jakarta, Jakarta
3) Industrial Engineering, Universitas Pembangunan Nasional Veteran Jakarta, Jakarta
4) Mechanical Engineering, Politeknik Negeri Bali, Bali

Corresponding email [1)] : zames@upnvj.ac.id

Abstract. Lithium-ion batteries need effective thermal management to avoid safety risks like thermal runaway. This study analyzes and optimizes a liquid cooling system. Battery Thermal Management System (BTMS) using a branching mini-channel cold plate design for eight Li-ion 18650 batteries. A Computational Fluid Dynamics model was developed to simulate performance at a 2C discharge rate with configurations of 3 (N3), 5 (N5), and 7 (N7) branches. The results, validated against experimental data, showed that all configurations kept maximum temperatures below 37°C and maintained temperature uniformity (ΔT) below 5°C. Increasing branches reduced pressure drop, with the N7 design showing the lowest ΔP of 5.16 Pa. Although it had a lower heat transfer coefficient, N7 achieved the highest J/F factor, indicating optimal thermo-hydraulic performance for liquid-cooled battery systems.

Keywords: BTMS, Branching Mini-Channel, Cold Plate, Li-Ion 18650, Liquid Cooling.

1. INTRODUCTION

In recent years, many studies have focused on energy sources, but continue to face challenges, mainly environmental pollution [1]. The G20 countries collectively account for about 76% of global greenhouse gas emissions, largely from natural resource use [2]. Advances in technology have encouraged the adoption of safer energy alternatives, such as batteries [3]. Cylindrical Li-ion batteries are particularly practical and widely applied in electric vehicles, backup systems, and small electronics [4]. However, their performance and safety remain sensitive to temperature variations [5]. Poor temperature control can cause thermal degradation, shorten service life, or even trigger thermal runaway and explosion [6].

Recent studies on battery cooling aim to reduce excessive heat generation in lithium-ion cells [7]. This effort led to the development of the Battery Thermal Management System (BTMS), designed to maintain optimal battery temperatures between 25°C-40°C and ensure temperature uniformity with $\Delta T < 5°C$ [8], [9]. The BTMS also enhances temperature homogeneity across all battery cells, extending cycle life and reducing operational costs [10], [11], [12]. Various configurations for BTMS have been suggested, such as systems utilizing air cooling, liquid cooling, phase change materials (PCM), and hybrid cooling methods [13]. Cooling strategies are generally categorized into active and passive systems. Among active approaches, liquid-based cooling is considered beyond effective than air cooling due to its superior heat removal and temperature stability [14], [15], [16]. Previous studies have examined liquid-cooling plates, as shown in Table 1.

Previous studies indicate that liquid cooling effectively reduces T_{MAX}, yet maintaining temperature uniformity (ΔT) remains challenging. Conventional serpentine designs face efficiency trade-offs under high discharge rates due to significant pressure drops (ΔP), while bionic channels introduce manufacturing complexity. Therefore, this study fills the gap in the research by numerically analyzes and optimizes a liquid-based BTMS using branching channel designs (3, 5, and 7 branches), considering branched designs offer an optimal balance between ease of manufacturing and high thermal performance. By optimizing the number of branches, this study hopes that simple geometries can compete with complex designs in maintaining battery temperature without complicated processes.

Table 1. Comparative Analysis of Previous Studies

Ref.	Author (s)	Configuration	Battery Type	Findings	Trade-offs
[17]	Ibrahim et al.	Serpentine Channel	18650 Cylindrical	Maintained T_{MAX} < 50°C (peak 46°C) and ΔT = 8.6°C at 2C discharge rate.	Failed to maintain ΔT < 5°C under higher discharge rates
[18]	Patil et al.	U-shaped Hexagonal	Pouch Cell	Inlet temperature affects T_{MAX} (99.31%), channel count affects ΔT (46.09%). Optimized ΔT reached 0.22°C.	Numerical sensitivity focus; specific geometry optimization required.
[19]	Li et al.	Hybrid (Heat pipe + Serpentine)	Prismatic	Significantly reduced ΔT by approximately 72.49% compared to standard plates.	Increased system complexity, weight, and manufacturing cost.
[20]	Wang et al.	Bionic Spider-web	Pouch Cell	Achieved T_{MAX} = 37.89°C at extreme 12C rate.	Poor temperature uniformity ΔT= 8.86°C exceeding the 5°C target.
[21]	Luo et al.	Square-Spiral-Ring	Prismatic	T_{MAX} = 33.63°C ΔT= 6.45 °C Pressure drop reduced by 686.8 Pa compared to serpentine.	ΔT remained above the ideal threshold of 5°C.
[22]	Wang et al.	Bionic Butterfly-shaped	Prismatic	Excellent uniformity ΔT = 4.99°C and low pressure drop (36.26 Pa vs. 189.11 Pa for serpentine).	Complex geometry leads to difficulty in manufacturability.

2. METHODS

2.1 Lithium-ion Battery Model

This research focuses on a liquid cooling system that has been designed explicitly for a cylindrical lithium-ion cell of the 18650 type. The arrangement of battery packs in terms of their thermal generation properties will be treated equally because the batteries are of the same type. The dimensions of the battery model are shown in Figure 1. It has a height of 65 mm and a diameter of 18 mm.

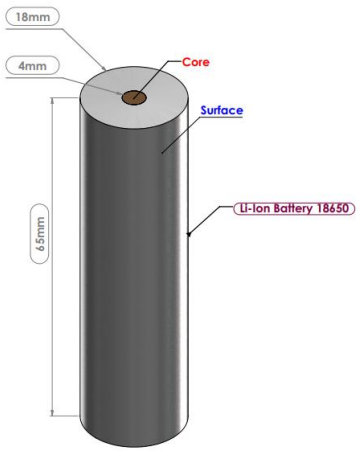

Figure 1. Lithium-ion 18650 battery model

2.2 Mini-Channel Cold Plate Models

Figure 2 illustrates the configuration of the batteries placed in a single module, followed by a visualization of the small channel branches inside the cooling plate. The liquid-based cooling configuration implemented consists of three different models: a three-branch, a five-branch, and a seven-branch mini-channel cold plate. There are eight battery arrays positioned in the cold plate. This configuration was chosen considering the liquid cooling strategy centered on mini-channels applied to induce forced convection. The cold plate component functions as the main source of heat exchange between the batteries and the fluid flow and is made of aluminum. The developed design also identifies key components such as the dimensions of the cold plate and the placement of the batteries.

Furthermore, Table 2 provides information on the material properties applied in this study including density, specific heat, thermal conductivity, and viscosity. Aluminum is utilized for the cold plate, while water serves as the cooling fluid.

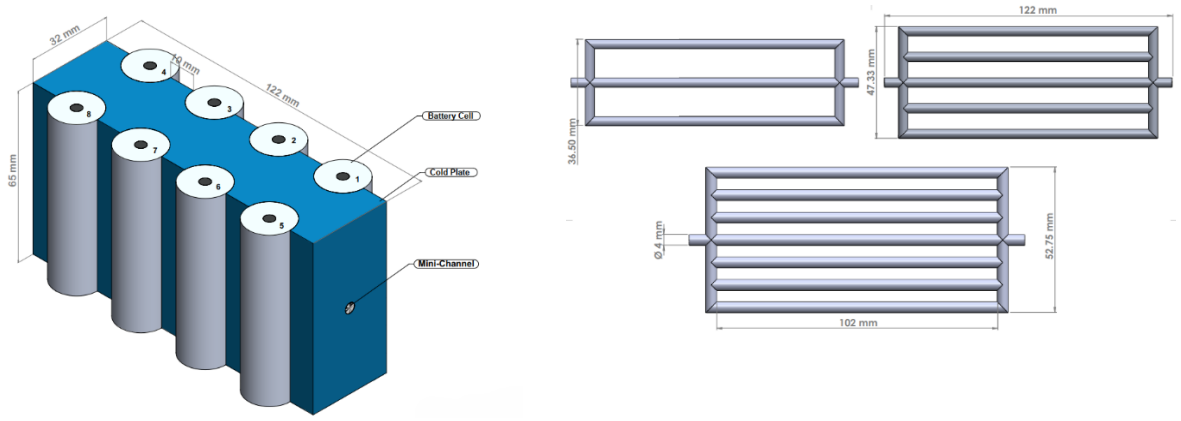

Figure 2. The structure of the branching mini-channel cold plate

Table 2. Thermal-physical Properties of the Battery Conditions

Material	ρ (kg.m^{-3})	c (J.kg^{-1}.k^{-1})	k (W.m^{-1}.k^{-1})	μ (Pa.s)
Alumunium	2179	871	202.4	-
Battery	2534.26	1558.3	3.02	-
Water	998.2	4128	0.6	1.03x10-3

2.3 Governing Equations

In this numerical study, a Computational Fluid Dynamics (CFD) solver is used. Then, to measure the interaction between the working fluid and the mini channel branching inside the cold plate, the concept of heat transfer is used because this phenomenon occurs to release heat from the battery. The mass flow rate applied to the cooling system design is defined as laminar flow. Therefore, fluid flow in this work utilizes the Navier-Stokes technique. To ensure that the fluid mass flow remains constant within the channel domain, equation (1), the Mass Conservation, is used to ensure that the fluid mass flow remains constant throughout the channel. Then, equation (2), momentum conservation, is used to measure the pressure distribution and velocity distribution along the flow moving within the channel. Equation (3) is functioned to model the phenomena of energy conservation and heat generation in batteries. Equation (4) is used to formulate a heat generation model based on the actual battery temperature conditions obtained from the experiment [23]. Furthermore, equation (5) is used to represent two heat generations to predict unsteady-state heat transfer in the battery, at locations in the core and surface of the battery.

$$\frac{\partial \rho}{\partial t} + \frac{\partial}{\partial x_i}(\rho u_i) = 0 \tag{1}$$

$$\rho_l \left[\frac{\partial \vec{v}}{\partial t} + (\vec{v} \bullet \nabla)\vec{v} \right] = -\nabla p + \mu \nabla^2 \vec{v} \tag{2}$$

$$\rho C_p \frac{\partial T}{\partial t} = \lambda_x \frac{\partial^2 T}{\partial^2 x} + \lambda_y \frac{\partial^2 T}{\partial^2 y} + \lambda_z \frac{\partial^2 T}{\partial^2 z} + Q_{gen} \tag{3}$$

$$Q_{gen}(t) = \rho C_p \frac{\Delta T}{\Delta t} \tag{4}$$

$$Q_{gen(1-2)}(x,y,z,t) = Q_{gen(1-2)}(t) - \lambda \nabla^2 T_{(1-2)} \tag{5}$$

2.4 Mesh and Boundary Conditions

An unstructured mesh in the shape of a tetrahedron was created in this study. This type of mesh is used because of its suitability for complex geometric shapes. The final mesh is shown in Figure 3(a). The variations used in this study are shown in Table 3, which shows the implementation of different numbers of channel branches in the

developed cooling model configuration. The channel diameter was fixed at 4 mm, and the mass flow rate was fixed at 0.0005 kg/s in each simulation case. The boundary conditions design is presented in Figure 3(b) , which consists of a battery, cold plate, and liquid zone. During the computational setup, the battery and aluminum cooling plate were set at a temperature of 35°C, following the ambient temperature experimental validation data for this article. Then, the initial water temperature was set at 25°C. Furthermore, a discharge rate of 2C was implemented in this case, considering the experimental data referred to, with heat generation applied as a heat source at radial gradient.

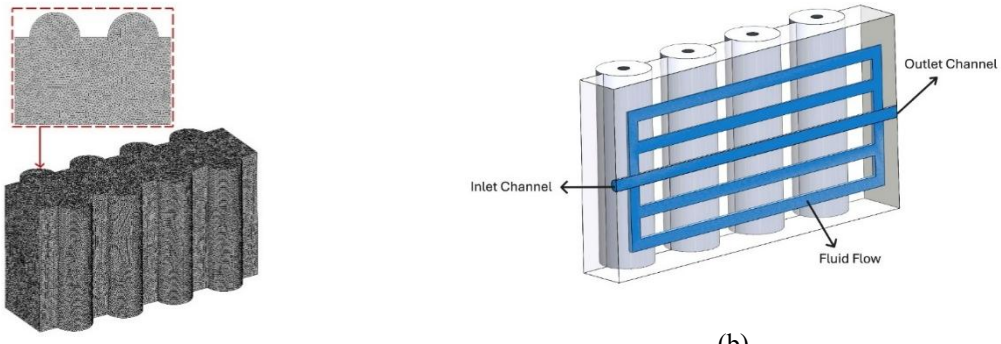

(a) (b)

Figure 3. The parameter specifications of this research: (a) mesh, (b) boundary conditions

Table 3. Parameter Variations in this Study

Number of channels (Branch)	Mass Flow Rate	Diameter Inlet (Ø)
3 Channel (N3) 5 Channel (N5) 7 Channel (N7)	0.0005 kg/s	4 mm

2.5 Non-dimensional Parameter

To expand the analytical understanding of the performance of the liquid cooling system implemented, this study adds a discussion on J/F, which is a non-dimensional factor number to calculate the performance efficiency approach. The non-dimensional parameter to measure the ability of fluids to transfer heat by convection is defined as the J factor, outlined in equation (6). Equation (7) is used to predict the flow regime, and equation (8) indicates the efficiency, the ratio of convective to conductive heat transfer across the boundary. The heat transfer rate, which is the measurement of thermal energy transfer per unit time, of the cold plate is quantified using equation (9). Equation (10) calculates the rate of heat absorption by the working fluid flow within the channel. The F factor, as a non-dimensional measure of pressure loss due to friction between the fluid and the channel walls, was evaluated using equation (11). Then, equation (12) calculates the pressure drop of the channel.

$$j = \frac{Nu}{Re \cdot Pr^{1/3}} \tag{6}$$

$$Re = \frac{\rho U D}{\mu} \tag{7}$$

$$Nu = \frac{h_w D}{\mu} \tag{8}$$

$$h_w = \frac{Q_l}{A_c[T_{bmax} - (T_{lin} + T_{lout})/2]} \tag{9}$$

$$Q = m.C_p.\ (T_{in} - T_{out}) \tag{10}$$

$$f = \frac{2\Delta p D c}{\rho_l U_{in}^2 L} \tag{11}$$

$$\Delta P = P_{in} - P_{out} \tag{12}$$

2.6 Mesh Independence Test

To ensure mesh quality, the estimation of numerical error for each mesh configuration was conducted using the Grid Convergence Index (GCI) method [24]. To calculate the ratio between the grid spacing of the fine mesh and the coarser mesh, using equation (13). Then, for determines how quickly the numerical error decreases as the grid is refined using equations (14). To calculate the uncertainty band error percentage for the fine and coarse mesh

used, indicating how far the result might be from the asymptotic true value (15) and (16), respectively, while the GCI reliability was verified through equation (18), and the benchmark value was used to calculate the true error of the simulation using equation (19). As summarized in Table 4, tests on battery 1, using its average temperature value, showed that the coarse, medium, and fine meshes contained 875,767, 1,751,435, and 3,502,671 elements, respectively. The fine mesh exhibited stable results with an error below 5%, confirming for subsequent analyses.

$$r = \frac{h_2}{h_1} \tag{13}$$

$$\overline{p} = \frac{\ln\left(\frac{f_3 - f_2}{f_2 - f_1}\right)}{\ln(r)} \tag{14}$$

$$GCI_{fine} = \frac{F_s \,|\in|}{\left(r^{\overline{p}} - 1\right)} \tag{15}$$

$$GCI_{coarse} = \frac{F_s \,|\in| \, r^{\overline{p}}}{\left(r^{\overline{p}} - 1\right)} \tag{16}$$

$$\in = \frac{f_{n+1} - f_n}{f_n} \tag{17}$$

$$\frac{GCI_{coarse}}{GCI_{fine} r^{\overline{p}}} \approx 1 \tag{18}$$

$$f\,\mathrm{r}_{h=0} = f_1 + \frac{(f_1 - f_2)}{\left(r^{\overline{p}} - 1\right)} \tag{19}$$

Table 4. Results of Mesh Independence Study.

Mesh	Fine	Medium	Coarse
Difference of Temperature	35.1546	35.1533	35.1493
$\overline{p}$		1.570096	
r		2	
GCIfine		0.002%	
GCIcoarse		0.0073%	
frh = 0		33.97114	
$\frac{GCI_{coarse}}{GCI_{fine} r^{\overline{p}}} \approx 1$		1	
Error	0.00196%	0.00581%	0.01724%

3. RESULTS AND DISCUSSION

3.1 Validation

To ensure validation can be used in this study, an experimental research approach model is required [23]. The aim is to bring the simulated battery temperature closer to actual conditions in the real world. The heat treatment applied to a single 18650 Li-ion battery included setting the ambient temperature at 35°C with a discharge rate of 2C. For more detailed results, see Figure 4. A close correlation was observed between the simulated and experimental data. Validation was performed by calculating the maximum deviations at the core and surface, which were 3.914% and 3.474%, respectively.

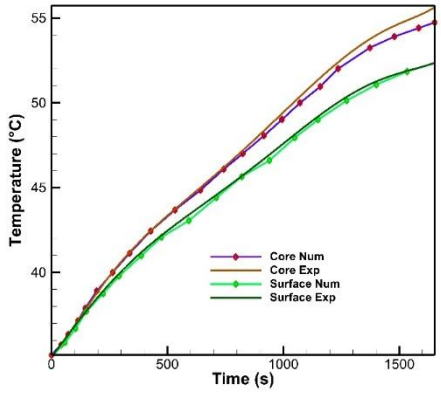

Figure 4. A comparison between numerical and experimental data on a single battery

3.2 Analysis

There are limitations to the model in this study, in which the battery computational domain used is arranged in series and parallel and only consists of eight units. Furthermore, the heat generation treatment in cylindrical batteries is given equally for all batteries, and the working fluid is incompressible. Furthermore, Figure 5(a) presents the evolution of T_{MAX} during discharge with and without mini-channel cold plates. Without active cooling, T_{MAX} rises rapidly and approaches 52°C by the end of the 1650-second simulation, underscoring the need for effective thermal management. With branched cold plates (N3, N5, and N7), the temperature rise is successfully controlled, with all configurations keeping T_{MAX} below 37°C after the initial peak at around 150 seconds. The differences among N3, N5, and N7 are minimal, only about 0.3°C at 900 seconds, because increasing the number of branches expands the heat-transfer surface and improves coolant distribution. Once steady operation is reached, the cooling system removes heat faster than the battery generates it, causing T_{MAX} to stabilize and gradually decline. The ΔT results, shown in Figure 5(b), indicate that all mini-channel configurations (N3, N5, N7) maintain excellent temperature uniformity, with values well below the 5°C threshold. The highest ΔT of about 2.4°C appears in N7, slightly higher than N3 and N5. This occurs because adding more branches lowers coolant velocity, briefly reducing convective heat transfer during early discharge. The ΔT increase in N7 is driven mainly by a drop in T_{MIN} rather than a rise in T_{MAX} , as the system cools faster than the battery equalizes heat internally.

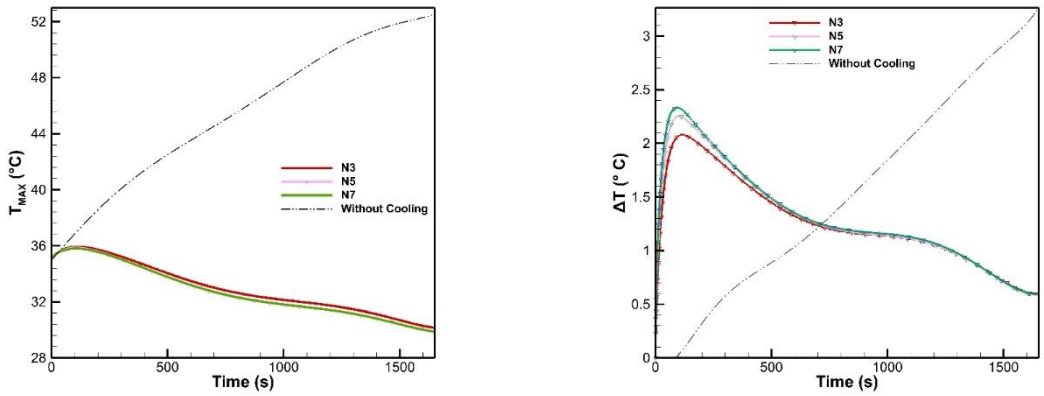

(a) (b)

Figure 5. Thermal response of the battery: (a) maximum temperature, (b) temperature difference for each configuration

Table 5 further shows that increasing the number of branches reduces pressure drop, from 6.42 Pa in N3 to 5.16 Pa in N7, indicating better hydraulic efficiency. However, the heat-transfer coefficient decreases with additional branching: N3 provides the highest value (624.59), while N7 delivers the lowest (291.32). Despite its larger ΔP, N3 still offers the strongest heat-transfer capability, demonstrating a practical performance trade-off.

Table 5. Pressure Drops and the Heat Transfer Coefficient with Each Configuration

Branching Channel	ΔP (Pa)	H_w (W $m^{-2}.K^{-1}$
N3	6.42	624.59
N5	5.50	391.32
N7	5.16	291.32

To evaluate the overall thermo-hydraulic accomplishment, Figure 6 presents the J/F analysis used to assess overall thermo-hydraulic performance by comparing heat-transfer effectiveness with the energy required to overcome frictional losses. The results show a steady increase in J/F as the number of branches grows. N7 delivers the highest value at about 0.21, followed by N5 at roughly 0.19, and N3 at around 0.17. This pattern indicates that the reduction in frictional losses outweighs the decrease in heat-transfer rate when the branches increase from 3 to 7. Consequently, the N7 configuration demonstrates the best overall thermo-hydraulic performance.

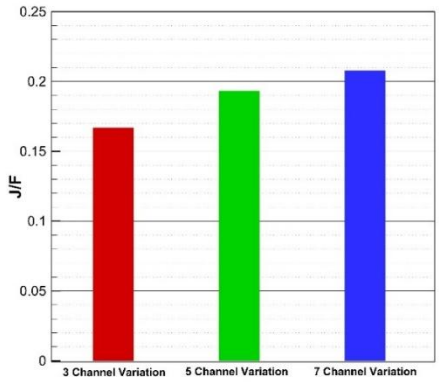

Figure 6. Thermal response of the battery for each configuration with the temperature difference

Figures 7, 8, and 9 collectively show that all configurations (N3, N5, N7) maintain good thermal uniformity at 1650 seconds, but N7 delivers the most compact high-temperature region. Physically, the N7 design increases the effective contact surface area and reduces the conduction path length between the battery surface and the coolant, facilitating more efficient heat extraction. Consequently, remaining hot spots are limited to areas outside the cold-plate contact zone, highlighting the geometric limitation where the cold plate does not fully envelop the battery cell. In contrast, N3 displays stronger temperature gradients due to fewer channels, which creates wider uncooled gaps between branches where heat accumulation occurs, while N5 performs at an intermediate level. Heat-flow contours further indicate that N7 provides the most uniform heat transport along the mini-channels, reducing local overheating and supporting better long-term battery stability. Pressure contours also reveal clear hydraulic differences: N3 experiences abrupt pressure changes as the flow splits into only three branches, increasing energy loss, whereas N7 maintains a lower-drop pressure distribution.

To apply this research to the real world, the right step for the battery manufacturing industry is to adopt a liquid cooling system design with branching channels so that it can be mass-produced. This is because, based on the above research results, the proposed cooling system for 18650 cylindrical Lithium-ion battery provides the best thermo-hydraulic performance balance and is able to maintain the battery temperature in the best condition and achieve temperature uniformity. With direct application in the real world, this means that the cooling pump requires less electrical power to circulate fluid in this cooling system. But the design needs to be further developed by expanding the cooling contact area and testing it under dynamic discharge rate conditions.

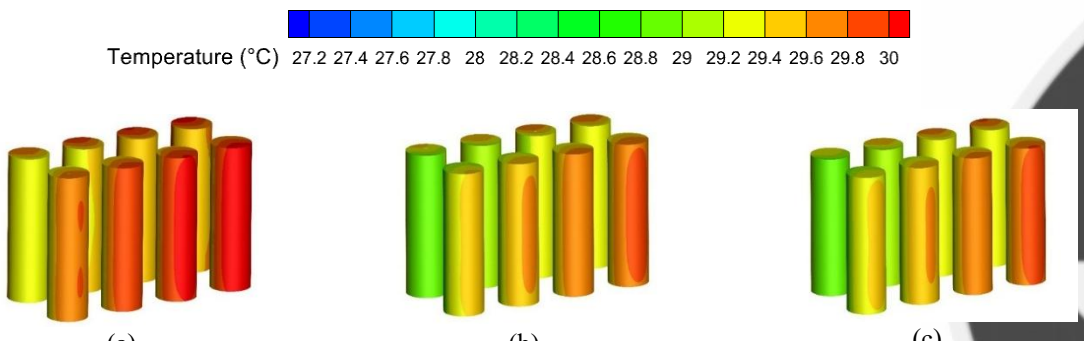

(a) (b) (c)

Figure 7. A comparison of thermal contour distribution of the battery (a) N3, (b) N5, (c) N7

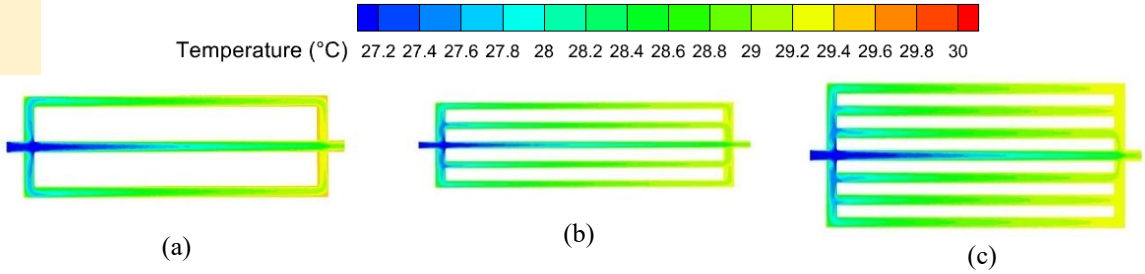

Figure 8. A comparison of branching mini-channel temperature distribution: (a) N3, (b) N5, (c) N7

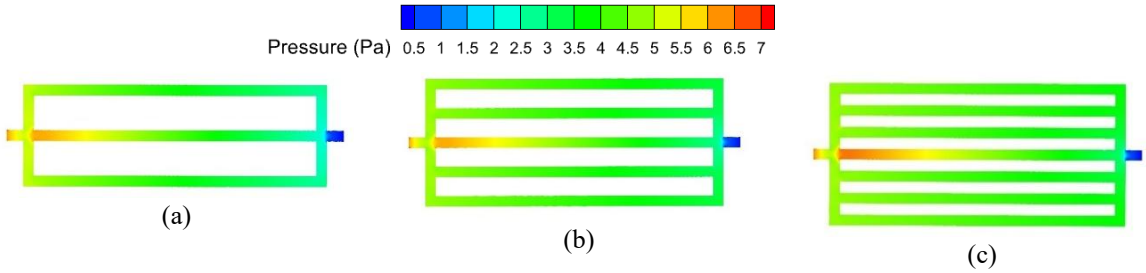

Figure 9. A comparison of branching mini-channel pressure distribution: (a) N3, (b) N5, (c) N7.

4. CONCLUSION

This numerical study examined the thermo-hydraulic behavior of a liquid-cooled BTMS using branching mini-channel cold plates for 18650 Li-ion batteries. All configurations (N3, N5, N7) successfully kept T_{MAX} below 37°C and maintained ΔT far under the 5°C threshold throughout discharge, meeting essential BTMS performance criteria. Increasing the number of branches lowered the pressure drop from 6.42 Pa (N3) to 5.16 Pa (N7), indicating reduced energy demand, though it was accompanied by a decline in the convective heat-transfer coefficient. Overall, N7 delivered the strongest and balanced performance, achieving the highest J/F value (0.21). This study has several limitations. The cooling plate design only uses side contact, so the battery poles and opposing surface rely on internal conduction, which causes hot spots outside the contact area. In addition, the analysis was performed at a constant discharge rate, so the transient thermal behavior under dynamic loads such as real driving cycles is still unknown. Future research should focus on improving the contact interface and evaluating performance under varied and realistic load profiles.

5. REFERENCES

[1] N. M. Malima, S. J. Owonubi, G. B. Shombe, N. Revaprasadu, and E. R. Sadiku, "Bioelectrochemical Technology for Sustainable Energy Production and Waste Treatment," in Bioelectrochemical Systems: Vol.2 Current and Emerging Applications, P. Kumar and C. Kuppam, Eds., Singapore: Springer, 2020, pp. 131–175. doi: 10.1007/978-981-15-6868-8_6.

[2] D. Murat, B. İnam, D. Murat, and B. İnam, "Relationship Between Fiscal Policies and Green Economy: An Application for G20 Countries," https://services.igi-global.com/resolvedoi/resolve.aspx?doi=10.4018/979-8-3693-2845-3.ch019. Accessed: Oct. 23, 2025. [Online]. Available: https://www.igi-global.com/gateway/chapter/www.igi-global.com/gateway/chapter/351395

[3] L. D. Tai and M.-Y. Lee, "Advances in the Battery Thermal Management Systems of Electric Vehicles for Thermal Runaway Prevention and Suppression," Batteries, vol. 11, no. 6, p. 216, June 2025, doi: 10.3390/batteries11060216.

[4] C.-L. Wang and J. C. Leong, "Analysis of Thermal Management Strategies for 21700 Lithium-Ion Batteries Incorporating Phase Change Materials and Porous Copper Foam with Different Battery Orientations," Energies, vol. 17, no. 7, p. 1553, Jan. 2024, doi: 10.3390/en17071553.

[5] N. Piao et al., "Challenges and development of lithium-ion batteries for low temperature environments," eTransp., vol. 11, 2022, doi: 10.1016/j.etran.2021.100145.

[6] Y. A. Bhutto, A. K. Pandey, R. Saidur, K. Sharma, and V. V. Tyagi, "Critical insights and recent updates on passive battery thermal management system integrated with nano-enhanced phase change materials," Materials Today Sustainability, vol. 23, p. 100443, Sept. 2023, doi: 10.1016/j.mtsust.2023.100443.

[7] F. A. Khalaf and A. L. Tarish, "Recent update progress for the battery thermal management of electric vehicles: challenges and solutions," Journal of Thermal Analysis and Calorimetry, vol. 150, no. 16, pp. 12135–12156, Aug. 2025, doi: 10.1007/s10973-025-14524-x.

[8] H. Tomar, S. Singh, P. Gupta, and K. Sireesha, "Design and Analysis of Thermal Management Systems for an Electric Vehicle Battery," in 2025 First International Conference on Advances in Computer Science, Electrical,

Electronics, and Communication Technologies (CE2CT), Feb. 2025, pp. 320–324. doi: 10.1109/CE2CT64011.2025.10941560.
[9] I. M. M. Benounnane, A. W. Belarbi, and M. E. B. Ghribi, "Comparative Analysis of Thermal Conductive Materials for Optimizing the Thermal Management of a Lithium-Ion Battery Pack," in 2024 3rd International Conference on Advanced Electrical Engineering (ICAEE), Nov. 2024, pp. 1–5. doi: 10.1109/ICAEE61760.2024.10783307.
[10] J. Zhao, P. Lv, and Z. Rao, "Experimental study on the thermal management performance of phase change material coupled with heat pipe for cylindrical power battery pack," Experimental Thermal and Fluid Science, vol. 82, pp. 182–188, Apr. 2017, doi: 10.1016/j.expthermflusci.2016.11.017.
[11] C. Wu, J. Ni, and X. Shi, "Research on multiple thermal conductivity phase-change-material-liquid thermal management system considering thermal safety and temperature uniformity of battery pack," Journal of Energy Storage, vol. 136, p. 118456, Nov. 2025, doi: 10.1016/j.est.2025.118456.
[12] M. Olyaei et al., "Virtual Testbed for Economical and Reliability Analysis of Battery Thermal Management Control Strategies1," Journal of Electronic Packaging, vol. 146, no. 041110, Aug. 2024, doi: 10.1115/1.4065988.
[13] A. Gharehghani et al., "Progress in battery thermal management systems technologies for electric vehicles," Renewable and Sustainable Energy Reviews, vol. 202, p. 114654, Sept. 2024, doi: 10.1016/j.rser.2024.114654.
[14] C. Wu, Z. Wang, Y. Bao, J. Zhao, and Z. Rao, "Investigation on the performance enhancement of baffled cold plate based battery thermal management system," Journal of Energy Storage, vol. 41, p. 102882, Sept. 2021, doi: 10.1016/j.est.2021.102882.
[15] A. Verma, T. Saikia, P. Saikia, D. Rakshit, and C. E. Ugalde-Loo, "Thermal performance analysis and experimental verification of lithium-ion batteries for electric vehicle applications through optimized inclined mini-channels," Applied Energy, vol. 335, p. 120743, Apr. 2023, doi: 10.1016/j.apenergy.2023.120743.
[16] Y. Chung and M. S. Kim, "Thermal analysis and pack level design of battery thermal management system with liquid cooling for electric vehicles," Energy Conversion and Management, vol. 196, pp. 105–116, Sept. 2019, doi: 10.1016/j.enconman.2019.05.083.
[17] A. Ibrahim, J. Guo, Y. Wang, Y. Zheng, B. Lei, and F. Jiang, "Performance of serpentine channel based Li-ion battery thermal management system: An experimental investigation," International Journal of Energy Research, vol. 44, no. 13, pp. 10023–10043, 2020, doi: 10.1002/er.5599.
[18] M. S. Patil, J.-H. Seo, S. Panchal, and M.-Y. Lee, "Numerical study on sensitivity analysis of factors influencing liquid cooling with double cold-plate for lithium-ion pouch cell," International Journal of Energy Research, vol. 45, no. 2, pp. 2533–2559, 2021, doi: 10.1002/er.5946.
[19] Y. Li, H. Guo, F. Qi, Z. Guo, M. Li, and L. Bertling Tjernberg, "Investigation on liquid cold plate thermal management system with heat pipes for LiFePO4 battery pack in electric vehicles," Applied Thermal Engineering, vol. 185, p. 116382, Feb. 2021, doi: 10.1016/j.applthermaleng.2020.116382.
[20] J. Wang, X. Liu, F. Liu, Y. Liu, F. Wang, and N. Yang, "Numerical optimization of the cooling effect of the bionic spider-web channel cold plate on a pouch lithium-ion battery," Case Studies in Thermal Engineering, vol. 26, p. 101124, Aug. 2021, doi: 10.1016/j.csite.2021.101124.
[21] W. Luo et al., "A numerical study of battery thermal management system with square spiral ring-shaped liquid cooling plate," Thermal Science and Engineering Progress, vol. 45, p. 102120, Oct. 2023, doi: 10.1016/j.tsep.2023.102120.
[22] Y. Wang et al., "Optimization of liquid cooling for prismatic battery with novel cold plate based on butterfly-shaped channel," Journal of Energy Storage, vol. 73, p. 109161, Dec. 2023, doi: 10.1016/j.est.2023.109161.
[23] N. Wang, A. Chen, W. Zhao, R. Zhu, and B. Duan, "An online temperature estimation for cylindrical lithium-ion batteries based on simplified distribution electrical-thermal model," Journal of Energy Storage, vol. 55, p. 105326, Nov. 2022, doi: 10.1016/j.est.2022.105326.
[24] P. J. Roache, "Perspective: A Method for Uniform Reporting of Grid Refinement Studies," J. Fluids Eng, vol. 116, no. 3, pp. 405–413, Sept. 1994, doi: 10.1115/1.2910291.